In Vivo Validation of a Propulsion Method for Untethered Medical Microrobots Using a Clinical Magnetic Resonance Imaging System

Jean-Baptiste Mathieu, *Student Member, IEEE*, Sylvain Martel, *Senior Member, IEEE*

***Abstract*— Models for MRI-based magnetic propulsion of untethered medical microrobots were validated both *in vitro* and *in vivo* using magnetic beads. In accordance with the theoretical models, a clinical MRI system has the capability to propel magnetic spheres with maximum velocity in blood vessels approximately twice the diameter of the device being navigated. The preliminary models were in accordance with data obtained in experiments performed in the carotid artery of a living swine where a 1.5mm sphere was propelled with a velocity of 13cm/s. These models were used in this paper to extrapolate the magnetic field gradients that will be required for propulsion and steering of magnetic particles and applicable for microrobots in blood vessels of various sizes, from the aorta to the capillaries.**

Index Terms—**Magnetic resonance imaging, magnetic particles, propulsion, *in vivo*, magnetophoretic velocity**

I. Introduction

THE use of Magnetic Resonance Imaging (MRI) gradient coils for magnetic actuation has been evaluated as a promising approach for navigation of wireless devices in deep tissues [1]. Such devices could have applications in the field of targeted delivery of drug carrying micro/nanoparticles or biosensors. In this optics, the MRI system becomes the main part of a robotic platform grouping magnetic actuation, tracking capabilities and real-time software orchestration for closed-loop control over the spatial distribution of the microdevices. Magnetic Resonance Propulsion (MRP) is based on the attraction force acting on a magnetized body and directed towards a position of higher magnetic field. The so-called magnetized body can be a ferromagnetic alloy or a superparamagnetic particle with magnetization M when placed in the field of an MRI system. The force acting on the magnetized body has a proportional dependence over the gradient (spatial variation) of the magnetic field according to:

$$\vec{F}_{mag} = \mu_0 . R . V . (\vec{M} . \nabla) \vec{H} , \qquad (1)$$

where, μ_0 is the vacuum permeability, R is the duty cycle of the gradient coils (time *on*/repetition time), V (m^3) and M (A/m) are respectively the volume and magnetization of the magnetized body, and H (A/m) is the magnetic field.

Until now, MRP experiments have been conducted mainly on millimeter-sized magnetic spheres with *in vitro* set-ups in order to validate macroscopic physical models [2-4]. More recently, a 1.5 mm sphere was controlled automatically inside the carotid artery of a living swine following a predefined 10 round-trips trajectory [5]. This experiment allowed our group to gather new MRP experimental data within real physiological conditions (viscous properties of blood at body temperature, friction coefficient and geometry of arterial walls). This paper presents two sets of experimental data. The first one is based on open-loop propulsion of a magnetic sphere on a Plexiglas plate and the second one refers to the *in vivo* experiments. These data are confronted with theoretical models which are then expanded towards MRP predictions in smaller vessels of the vascular system. These predictions will be used as design guidelines for propulsion dedicated magnetic gradient coils inserts for MRI systems.

II. Materials and Methods

A. Magnetic Resonance Propulsion

The sequence of events involved in MRP is the following. A fast tracking imaging scheme based on *off resonance* projections is executed [6]. Three projections of the volume of interest which shape depends on the position of the ferromagnetic sphere are acquired. This information is fed to dedicated software [7] which computes the current position by cross correlation based on previous data. In order to obtain closed-loop position control, the measured position is compared to the desired position and a PID controller is used to compute the amplitude and direction of the magnetic force to apply [8]. The adequate propulsion force is then applied by the scanner on the sphere and the control loop starts again. This sequence of events is schematically depicted in Fig 1. Nevertheless, in actual experiments, the computation and propulsion phases take place simultaneously in order to optimize the refresh rate of the system.

Manuscript received March 28, 2007. This project is supported in part by the Canada Research Chair (CRC) in Micro/Nanosystem Development, Fabrication and Validation, the Canada Foundation for Innovation (CFI), the National Sciences and Engineering Research Council of Canada (NSERC), Fonds Québécois de la Recherche sur la Nature et les Technologies (FQRNT), and the Government of Québec.

J.B. Mathieu and S. Martel are with the NanoRobotics Laboratory, Computer Engineering Department, École Polytechnique de Montréal (EPM), Montréal (Québec) Canada, H3C 3A7, (corresponding author: Sylvain Martel, phone: 514-340-4711 #5029; fax: 514-340-5280; e-mail: sylvain.martel@polymtl.ca, jean-baptiste.mathieu@polymtl.ca).

B. Magnetic Sphere and MRI System Gradients

A ferromagnetic 1.5 mm (0.0136 grams) diameter chrome steel sphere (Table I) is considered. Its magnetization $M_{1.5T}$ = 1.35 × 10^6 A/m was measured using a VSM at B_0 = 1.5 T being the field present inside the bore of the MRI system used. This chrome steel alloy was chosen because of its high saturation magnetization and availability in spherical shape with a wide range of diameters. Maximum gradient amplitude generated by the MRI system is 40 mT/m. Maximum duty cycle at 40 mT/m is 44.5 % and was determined by trial and error. This leads to a usable gradient of 17.8 mT/m.

C. In vitro Data

In vitro propulsion data were acquired to validate the theoretical models. A magnetic sphere was propelled on a horizontal Plexiglas plate along the x and z horizontal directions of the MRI system. Its position was recorded using a custom MR tracking method [6]. The sphere can roll along x while it slips along z [3]. A second Plexiglas plate was placed 3 mm above the first one to prevent the sphere from being lost in the MRI tunnel. Water density and viscosity values of 0.998 g/cm^3 and 1.0 cp respectively were used in simulations.

D. In vivo Data

The sphere position was recorded with a refresh rate of 24 Hz (41.6 ms repetition time) in this particular experiment. An inner diameter of 5 mm of the carotid artery was measured from MRI and X-ray images. Blood was considered as a monophasic fluid and density and viscosity values of 1.05 g/cm^3 and 3.5 cp respectively [9] were used in simulations.

E. Animal Preparation

One 6-F, 80 cm introducer catheter was inserted through a right femoral approach into the proximal portion of the right carotid artery under fluoroscopic guidance. A 5 mm × 18 mm angioplasty balloon was advanced under fluoroscopic guidance in the distal portion of the right common carotid artery (10 cm downstream to the tip of the long introducer) over a 0.018" guide wire (Fig.2). The introducer catheter was used as the release route for the magnetic sphere to be controlled whereas the balloon catheter was used to control the flow and eventually block the sphere in order to facilitate its retrieval at completion of control experiments.

F. Free Sphere Introduction, Release and Closed-loop Navigation

The 6-F inner dilator catheter of the long introducer catheter was cut at its distal portion and used to push a chrome steel sphere inside the long introducer. The sphere was brought in pre-release position 15 mm above the distal tip of introducer *A* using a color marking on the inner dilator as a visual landmark.

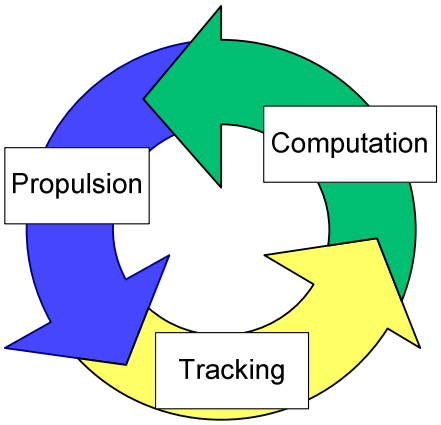

Fig. 1. Schematic description of an MRP feedback loop.

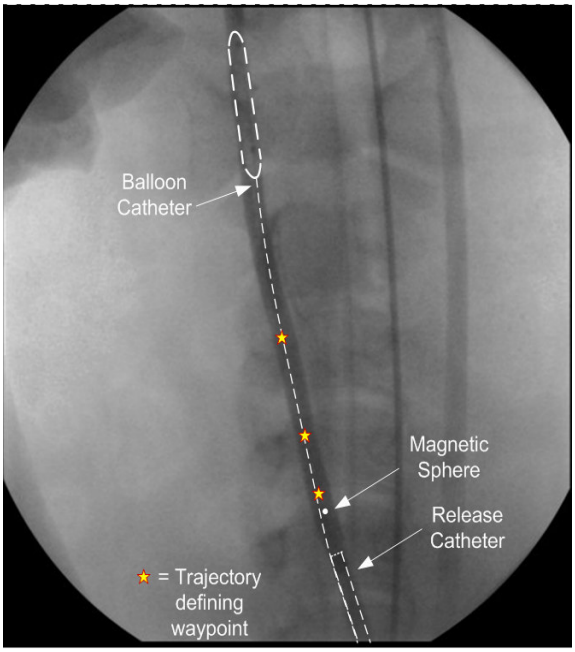

Fig. 2. X-ray angiogram of the right carotid artery of the animal showing catheter placement. Stars indicate the position of the trajectory defining waypoints and white dot illustrates the magnetic sphere that was navigated.

TABLE I
LIST OF MANUFACTURERS

Material	Manufacturer
Magnetic sphere	Salem Specialty Balls Company, Canton, CT, USA
VSM	Walker Scientific VSM, Worcester, MA, USA
MRI system	Siemens Magnetom Avanto 1.5 T, Erlangen, Germany
Fluoroscopic system	HICOR/ACOM-TOP, Siemens, Erlangen, Germany
Ultrasound system	GE VingMed Ultrasound Vivid Five, 10 MHz probe
Introducer catheter	Cook, Bloomington, Indiana
Balloon catheter	AV100, Medtronic, Santa Rosa, CA
Magnetic tipped catheter	Terumo, Somerset, NJ, USA

The balloon catheter was inflated to prevent the sphere from being carried away in case of unplanned problem. The real-time feedback control sequence was started. Using custom software, the position of the sphere was visualized in real-time in the scanner's room in order to allow the clinician to monitor the release of the sphere and the control procedure.

The sphere was released by pushing the dilator all the way through the long introducer. Once the sphere was released, its movement was dealt with by the feedback control sequence using a PID controller which objective was to navigate it through a preplanned trajectory. Position data and command magnetic gradients were continuously saved.

Retrieval of the sphere from the carotid artery was performed using a custom built magnetically tipped catheter (based on a glidecath 5-F catheter) under TRUFI_IRTTT, a real time imaging sequence from Siemens.

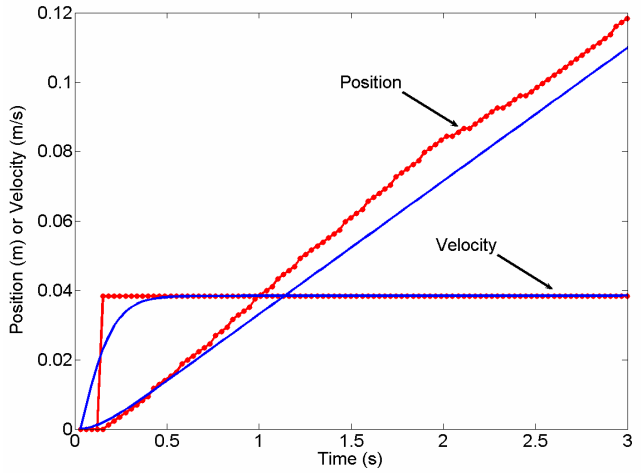

Fig. 3. Position and velocity data for *in vitro* propulsion along the *x* axis of the MRI system. Solid lines are from simulations while dotted lines show experimental data points. Propulsion gradient was 10 mT/m, duty cycle was 46 % and a 0.056 rolling friction coefficient was used for simulation.

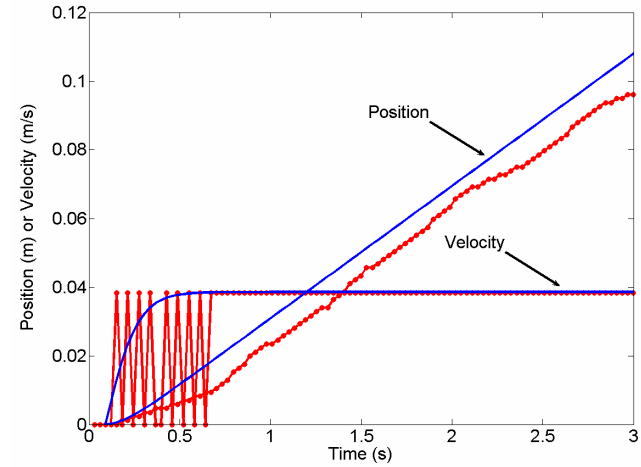

Fig. 4. Position and velocity data for i*n vitro* propulsion along the *z* axis of the MRI system. Solid lines are from simulations while dotted lines show experimental data points. Propulsion gradient was 26 mT/m, an upward 25 mT/m gradient was applied to reduce friction, duty cycle was 46 % and a 0.25 dynamic friction coefficient was used for simulation.

At the end of the procedure, the animal was euthanized with 19 ml of Euthanyl Forte Bimeda 5 mg/ml injected over a period of 15 minutes.

G. Theoretical Model

The model of [2] was used with minor differences. In [2] MRP was investigated in a vertical tube. In the present paper a friction force was modelled to take the contacts between the sphere and the tube walls into account. The second difference lies in the choice of the correlation for the retarding effect of vessels walls. Here, correlation from [10] was used since it is valid for Reynolds numbers from 0 to 2×10^5 which makes it usable both for validation of the model at millimeter scale and for MRP predictions at microscale. Even though the sphere moved between two parallel flat plates instead of inside a cylindrical tube during the *in vitro* tests, the same wall effect correlation was used for model validation.

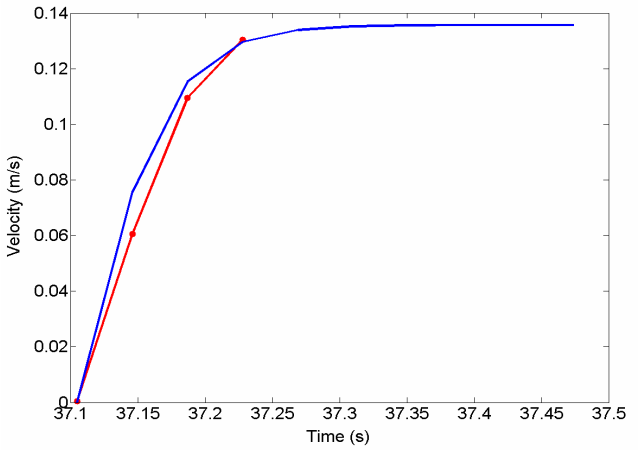

Fig. 5. Velocity data for i*n vivo* along the *z* axis of the MRI system. Solid line is from simulations while dotted line shows experimental data points. Propulsion gradient was 40 mT/m, an upward 30 mT/m gradient was applied to reduce friction, duty cycle was 44.5 % and a 0.094 dynamic friction coefficient was used for simulation.

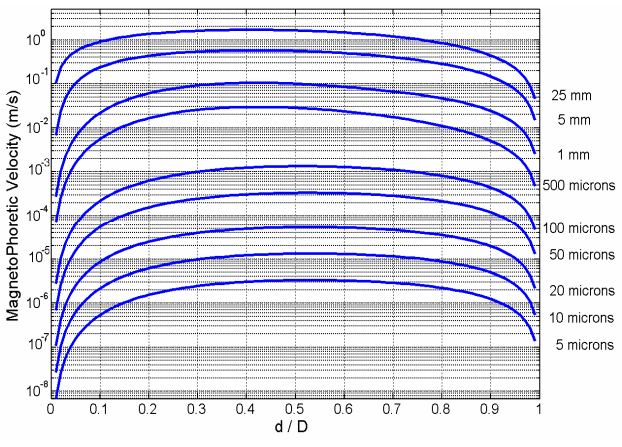

Fig. 6. Magnetophoretic velocity prediction of Permendur particles in various blood vessels under the influence of a 400 mT/m propulsion gradient

III. Results

In vivo and *in vitro* magnetic sphere navigation data were correlated with command gradients and compared with theoretical predictions based on magnetic and drag force balance models as described in [2].

Figure 3 and Fig. 4 show *in vitro* position and velocity data along the x and z axis of the MRI system respectively. Experimental and simulation data show good agreement with realistic rolling and slipping friction coefficients values. The sawtooth aspect of the experimental velocity data of Fig. 4. is attributed to the limited resolution of the tracking method which tends to make the curve noisy.

As for the *in vivo* experiment, the control software was able to navigate the sphere and to accomplish ten roundtrips through the trajectory defining waypoints as was preprogrammed for this demonstration.

Few data points are available for *in vivo* propulsion. As a matter of fact, these data come from closed-loop control experiments where the gradient changed in real-time and was likely to vary between consecutive acquisition points. The data points depicted in Fig. 5 were chosen because a constant command gradient of 40 mT/m was applied for each point. Moreover, they show acceleration from 0 m/s to the maximum velocity achieved during the control experiment (13 cm/s). Such an acceleration curve is adequate for validation of propulsion models purposes. Once again, good agreement between experimental and simulation data is found. Dynamic friction coefficient value of 0.094 is from [11].

Once validated in a physiological environment, the theoretical model was used to predict the magnetophoretic velocities in blood of magnetic particles composed of 50 % volume of Permendur (M_{Sat} = 1.95×10^6 A/m) under a gradient increased by a ten fold factor: ∇B_{sim} = 400 mT/m. Such gradient amplitude could be achieved by developing specialized gradient coil inserts with high gradient amplitude prevailing over inductance and linearity as the dominant design requirement.

In Fig. 6, the magnetophoretic velocity of different magnetic particles was computed as a function of the ratio *d/D* of particle diameter over vessel diameter for various blood vessels from the aorta (25 mm dia.) to the smallest capillaries (5 μm dia.). In the case where several magnetic particles form aggregates, the hydrodynamic diameter of the aggregate is used as diameter *d*. One can see that for a given vessel, the maximum magnetophoretic velocity occurs for a *d*/D ratio between 0.4 and 0.5. For smaller particles, the drag forces are comparatively higher than the magnetic force. As for bigger particles, the retarding effect of the vessels walls become predominant and reduces the magnetophoretic velocity.

IV. Discussion

The choice of the 1.5 mm chrome steel sphere for closed-loop control experiments inside the carotid artery of a living swine was the result of a trade-off between different aspects of the project. It is an example of the methodologies and constraints that will have to be dealt with for microparticles navigation and design for future applications. The first constraint is the 5 mm lumen of the carotid artery of the animal that sets an upper limit to the diameter of the sphere. The lower size limit was dictated partly by the maximum amplitude and duty cycle of the magnetic gradient that could be generated and partly by tracking signal quality considerations. Gradient amplitude constraints required the sphere to be in the millimeter range in order to allow any possibility of sustaining the expected blood velocity in the artery (average blood velocity of 7 cm/s had been measured on another animal prior to the actual tests). As for tracking, a low quality signal could have impeded the whole control experiment. Since SNR is proportional to the magnetic moment of the sphere (R^3 dependency) a millimeter sized sphere was chosen in order to stay on the safer side. Three doppler ultrasound flow measurements were assessed for three different inflation volumes of the balloon catheter namely (0cc, 0.3cc, 0.5cc) on the day of the actual *in vivo* control tests. The corresponding average blood velocities were respectively 20.2 cm/s, 8.52 cm/s and 0 cm/s. Due to this high flow compared to the expected value of 7 cm/s, the control experiments were performed while the balloon catheter was fully inflated to guarantee the success of the procedure. The high variability in blood velocity measurements among different subjects underlines the need for higher propulsion gradient amplitude than required to ensure the reliability of MRP based applications.

Figure 5 shows that the assumption of blood being a monophasic fluid holds at millimeter scale. In this paper, blood was modeled as a monophasic flow even for microcirculation vessels. The validity of this assumption could be questioned at microscale. Modeling of blood rheological behavior is a complex field and is beyond the scope of this paper. As a matter of fact, our objective is to give design guidelines for propulsion gradient coils rather than to provide exact modelization of the interactions of microparticles with blood constituents. We expect that microparticle being propelled in blood will travel between blood cells through blood plasma which has a lower viscosity and density than whole blood. Therefore, we believe that considering blood as a monophasic fluid with the fluidic properties of whole blood to be a conservative and helpful design hypothesis in the context of this paper.

From Table II, blood velocity is between 0.5 and 1 mm/s in a 10 μm diameter 1 mm long human capillary [12,14]. From Fig. 6, one can see clearly that a 400 mT/m gradient is not sufficient to allow a microparticle to sustain such a flow. Nevertheless, one can let the blood flow drive the particles in the vascular bed and control them by using magnetic force in order to guide their trajectory. Microcirculation can be

regarded as a redundant branching vascular network. Particles can be steered in each vessel of this network towards a preferred outlet at the next bifurcation [15]. In a 5 – 10 µm capillary, such strategy requires a magnetophoretic velocity of 1.25 - 5 µm/s for a particle to cross the radius of the vessel in the 1 to 2 second time window required for blood to flow through it. From Fig. 6, one can see that particles or aggregates with diameter comprised between 1.8 µm and 9 µm in a 10 µm capillary can reach a higher velocity than 5 µm/s using 400 mT/m.

In future medical applications, it is likely that particles will be injected in larger vessels upstream to the targeted organ. Hence, particles being small enough to travel in the microcirculation will probably be too small to be steered in these larger vessels. Restraining blood flow is not an optimal approach to cope with this constraint. The solution to this practical problem might come from the aggregation behavior of the magnetic particles.

During preliminary experiments in MRI, it was observed that once magnetized the 10.8 µm diameter Fe_3O_4 particles contained in a distilled water suspension formed needle shaped aggregates that occupied the major part of the tubes they were flowing into (Fig.7.). More interestingly, when tube diameter changed, these aggregates would dissolve and reorganize in order to comply with the new geometry of the channel.

TABLE II
PHYSIOLOGICAL PARAMETERS OF HUMAN VASCULAR SYSTEM

References * [12] ** [13] *** [14]	Diameter	Length	Blood velocity max	Blood velocity average
	m	m	m/s	m/s
Ascending aorta	2.10^{-2} $3.2.10^{-2}$ ***		0-1.12 ** 0.63 ***	0.18 **
Aorta	$2.5.10^{-2}$ *	0.5 *		
Abdominal Aorta	$1.6.10^{-2}$-2.10^{-2} ***		0-0.75 ** 0.27 ***	0.14 **
Larger arteries	2.10^{-3}-6.10^{-3} ***		0.20-0.50 ***	
Arteries	4.10^{-3} *	0.5 *		
Renal artery			0.26-0.73 **	0.40 **
Femoral artery			0.02-0.52 **	0.12 **
Arterioles	50.10^{-6} *	1.10^{-2} *		
Precapillary phincter	35.10^{-6} *	$0.2.10^{-3}$ *		
Capillary	8.10^{-6} * 5.10^{-6}-1.10^{-6} ***	1.10^{-3} *		$0.5.10^{-3}$-1.10^{-3} ***
Venules	20.10^{-6} *	2.10^{-3} *		
Veins	5.10^{-3} *	0.25 *		
Larger veins	5.10^{-3}-10^{-2} ***			0.15-0.2 ***
Vena cava	$2.0.10^{-2}$ *** $3.0.10^{-2}$ *	0.5 *		0.11-0.16 ***

Nevertheless, even though aggregates could help enhance the steering efficiency by increasing the magnetophoretic velocity in larger vessels, they could also cause problems when getting too large. First, velocity of the larger aggregates would be restrained by the wall retardation effect. Second, a large aggregate reaching a bifurcation is likely to break evenly between the two branches which would void the steering effort.

Aggregate size and shape is influenced by several parameters such as particle size, magnetization, concentration, surface properties as well as magnetizing field amplitude or viscous or ionic properties of the surrounding fluid. Tuning of these parameters could allow the design of magnetic suspension which aggregation properties would be tailored to optimize the steering efficiency from injection site in larger vessels to the smaller vessels of the targeted area.

A next step would be to further refine the models proposed here in order to take interparticles interactions into account.

V. CONCLUSION

The use of an MRI system as actuation method for magnetized particles and robotic platform has been validated in physiological conditions. Due to scaling laws, additional magnetic gradient coils with an order of magnitude increase in amplitude will have to be designed.

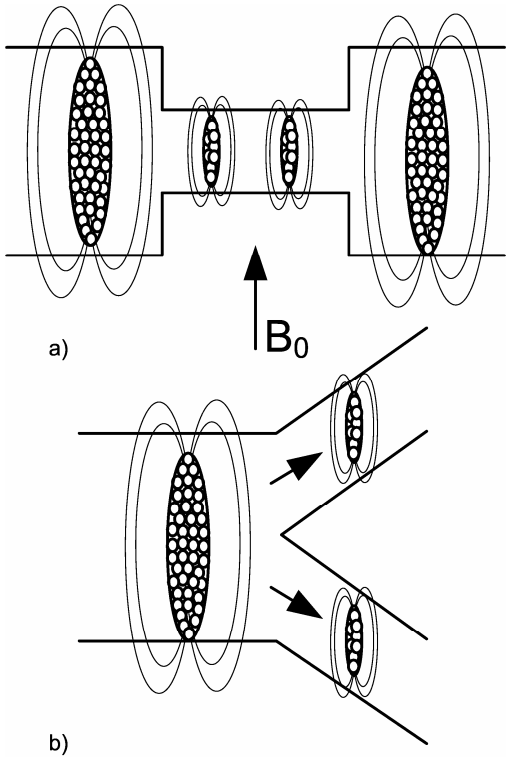

Fig. 7. Flowing behavior of magnetic particles aggregates. Field lines are schematically represented around aggregates. Needle shaped aggregate aligned with B_0 field flow side by side because of repulsion forces. a) Larger aggregate complies with channel size restriction. b) Large aggregate splits evenly between both outlets of branching channel.

Their purpose will be to generate sufficient propulsion forces to propel magnetic microparticles against the viscous forces encountered in the microcirculation. Particle size is a crucial parameter. It appears from the MRP models that with a given maximum magnetic gradient, a single particle cannot be adapted for navigation in all the vessels from the aorta to smaller size particles to be controlled in larger vessels. These agglomerates would have to break apart in order to comply with smaller vessels diameters. Such reversible aggregates could either be composed of magnetic particles embedded in a polymer with rapid biodegradability kinetics of they could be made up of magnetically aggregating particles.

Optimized magnetic particles suspensions, propulsion dedicated gradient coils, deformable magnetic disturbance tracking methods and learning control software add-ons have been identified as the next steps in the adaptation of our MRI based robotic navigation platform from millimeter sized spheres to microparticles agglomerations.

ACKNOWLEDGMENT

The authors acknowledge assistance from Dr. Gilles Soulez for his help in designing the in vivo experimental protocol, Gilles Beaudoin for his help with MRI sequences and Ouajdi Felfoul, Arnaud Chanu, Eric Aboussouan, Pierre Pouponneau, Samer Tamaz and Martin Mankiewicz, without whom these experiments could not have been conducted.

REFERENCES

[1] S. Martel, J.-B. Mathieu, O. Felfoul, H. Macicior, G. Beaudoin, G. Soulez, and L. Yahia, "Adapting MRI Systems to Propel and Guide Microdevices in the Human Blood Circulatory System," *26th Conference of the IEEE Engineering in Medicine and Biology Society ,* San Francisco, 2004.

[2] J. B. Mathieu, G. Beaudoin, and S. Martel, "Method of propulsion of a ferromagnetic core in the cardiovascular system through magnetic gradients generated by an MRI system *IEEE Transactions on Biomedical Engineering*," vol. 53, no. 2, pp. 292-299, 2006.

[3] J.-B. Mathieu, S. Martel, L. Yahia, G. Soulez, and G. Beaudoin, "Preliminary Investigation of the Feasibility of Magnetic Propulsion for Future Microdevices in Blood Vessels," *BioMedical Materials and Engineering*, vol. 15, pp. 367-374, 2005.

[4] J.-B. Mathieu, S. Martel, L. Yahia, G. Soulez, and G. Beaudoin, "MRI Systems as a Mean of Propulsion for a Microdevice in Blood Vessels," *IEEE Engineering in Medicine and Biology Society ,* Cancun , pp. 3419-3422, 2003

[5] S. Martel, J. B. Mathieu, O. Felfoul, A. Chanu, E. Aboussouan, Tamaz, S., P. Pouponneau, G. Beaudoin, G. Soulez, L. Yahia, and M. Mankiewicz, "Automatic navigation of an untethered device in the artery of a living animal using a conventional clinical magnetic resonance imaging system," *Applied Physics Letters*, vol. 90, 10, Mar 12, 2007.

[6] O. Felfoul, J. B. Mathieu, G. Beaudoin, and S. Marte1, "MR-Tracking Based on Magnetic Signature Selective Excitation," *IEEE Trans. Med. Im.*, Accepted Feb 4, 2007.

[7] A. Chanu, O. Felfoul, S. Tamaz, J. B. Mathieu, G. Beaudoin, and S. Martel, "Adapting MRI for the Real-Time Navigation of Endovascular Untethered Ferromagnetic Devices," *Magnetic Resonance in Medicine*, Accepted May 6, 2007.

[8] S. Tamaz, R. Gourdeau, A. Chanu, J. B. Mathieu, and S. Martel, "Real-time MRI-based Control of a Ferromagnetic Core for Endovascular Navigation," *IEEE Transactions on Biomedical Engineering*, Accepted with minor revisons.

[9] K.B. Chandran. *Cardiovascular Biomechanics*, New York University Press, 1992.

[10] R. Kehlenbeck and R. Di Felice, "Empirical Relationships for the terminal Settling Velocity of sheres in cylindrical Columns," *Chemical Engineering Technology*, vol. 21, 4, pp. 303-308, 1999.

[11] K. Takashima, R. Shimomura, T. Kitou, H. Terada, K. Yoshinaka, and K. Ikeuchi, "Contact and Friction between Catheter and Blood Vessel," *Tribology International*, vol. 40, no. 2 SPEC ISS, pp. 319-328, 2007.

[12] Charm S.E. and Kurland G.S. *Blood Flow and Microcirculation*, John Wiley & Sons, 1974.

[13] Milnor, W. R. *Hemodynamics*, Baltimore/London: Williams and Wilkins, 1982.

[14] R.L. Whitmore. *Rheology of the Circulation*, Pergamon Press, 1968.

[15] J.B. Mathieu and S. Martel, "Magnetic Steering of Iron Oxide Microparticles Using Propulsion Gradient Coils in MRI," *28th Conference IEEE Engineering in Medicine and Biology Society (EMBS),* NYC USA, p 472-475, 2006.